Computing 64, 97–122 (2000)

Computing

Multilevel Gauging for Edge Elements*

R. Hiptmair, Tübingen

Received May 27, 1999; revised October 22, 1999

Abstract

The vector potential of a solenoidal vector field, if it exists, is not unique in general. Any procedure that aims to determine such a vector potential typically involves a decision on how to fix it. This is referred to by the term gauging. Gauging is an important issue in computational electromagnetism, whenever discrete vector potentials have to be computed. In this paper a new gauging algorithm for discrete vector potentials is introduced that relies on a hierarchical multilevel decomposition. With minimum computational effort it yields vector potentials whose L^2-norm does not severely blow up. Thus the new approach compares favorably to the widely used co-tree gauging.

AMS Subject Classifications: 65N30, 65N55, 78A30.

Key Words: Computational electromagnetism, edge elements, hierarchical bases, multilevel decomposition, vector potentials, gauging.

1. Introduction

A common problem in magnetostatics is the computation of a magnetic field $\mathbf{H}$ satisfying

$$\begin{aligned} \mathbf{curl}\,\mathbf{H} = \mathbf{j} \quad &\text{and} \quad \operatorname{div}\mu\mathbf{H} = 0 \ \text{ in } \Omega \\ \mathbf{H}\times\mathbf{n} = 0 \ \text{ on } \Gamma_D \subset \partial\Omega \quad &\text{and} \quad \langle \mathbf{H},\mathbf{n}\rangle = 0 \ \text{ on } \Gamma_N \subset \partial\Omega. \end{aligned} \tag{1}$$

The exciting current $\mathbf{j}$ is supposed to be divergence-free with vanishing flux through Γ_D. Originally, the problem is posed on the entire space $\mathbb{R}^3$, but through exploiting symmetry, idealized materials ("magnetic walls") and artificial cut-off boundaries the above boundary value problem emerges. If Ω is simply connected – often rendered so by introducing cutting surfaces [37] – (1) can be converted into a second order elliptic problem for a scalar magnetic potential, as soon as a field $\mathbf{H}_0$ is known satisfying $\mathbf{curl}\,\mathbf{H}_0 = \mathbf{j}$. This is where the problem of computing a vector potential for the solenoidal vector field $\mathbf{j}$ pops up. It also occurs outside magnetostatics in the realm of eddy current computation, if the so-called $\mathbf{A}$-V ($\mathbf{B}$-oriented)-formulation [2] is used. A comprehensive exposure of the use of potentials in computational electromagnetism is given in [14, 17].

* This work was supported by DFG as part of SFB382.

Of course, cohomology theory teaches that, in general, it is only possible to find such $\mathbf{H}_0$, if Ω has a special topology marked by the absence of cavities. If, in addition, we require $\mathbf{H}_0 \times \mathbf{n} = 0$ on Γ_D, its existence depends on the arrangement of the connected components of Γ_D. In any case, there is a cohomology space $\mathscr{H}_2$ of small dimension, such that for some $\mathbf{h} \in \mathscr{H}_2$ the difference $\mathbf{j} - \mathbf{h}$ is a **curl** [3, 37].

One way to get $\mathbf{H}_0$ is by Biot-Savart's law [36]. It is ideally suited for simple current loops, but the treatment of complicated spatial currents is hardly feasible computationally. Numerical techniques starting from an approximation of $\mathbf{j}$ are the only available option then. The non-uniqueness of the vector potential confronts us with an abundance of choices. Strictly speaking, we seek an equivalence class of vector potentials [38], but for numerical purposes we have to employ some "gauging" by selecting a representative. A guideline for the choice of $\mathbf{H}_0$ is offered by the fact that the final solution $\mathbf{H}$ of (1) has to be computed by adding a correction to $\mathbf{H}_0$. In case $\mathbf{H}_0$ is "huge" (in terms of norm or discrete coefficients) compared to $\mathbf{H}$ severe cancellation will occur [14, Section II.B.2], potentially rendering the result meaningless. Hence it must be one objective to *determine a vector potential of small norm*. We can achieve this by the Coulomb gauge $\operatorname{div} \mathbf{H}_0 = 0$ (a "metric gauge" in the parlance of [38]), but at the expense of solving a full boundary value problem, which usually carries a high price tag. Thus, we are looking for a cheaper way to come up with satisfactory gauging.

The issues of gauging and discretization are inextricably intertwined. A physically sound and increasingly popular way of discretizing electromagnetic quantities is by *discrete differential forms* (see [15, 16, 47] and, in particular, [17] for a lucid presentation) that perfectly match the continuity properties of the fields. Thus a discrete 2-form should be used to describe the current $\mathbf{j}$, whereas the vector potential will be a discrete 1-form. Discrete differential forms give rise to finite element spaces, known as spaces of Whitney-forms. The crucial property of these spaces, apart from making the differential operators well defined, lies in the existence of discrete potentials, topology permitting.

A popular way to construct a unique vector potential for a lowest order discrete 2-form relies on so-called *spanning tree techniques*, first explored in circuit analysis and made popular by Albanese and Rubinacci [1]. Its foundation is a graph theoretic treatment of the finite element mesh. For a general exposition we refer to [17, Section 5.3] and latest developments for more complex topologies can be found in [37, Section 4]. However, this technique is purely algebraic and it is hard to control the norm of the computed vector potential. A more thorough discussion of this point will be postponed to section three.

What are practical alternatives? After we have computed a vector potential $\mathbf{H}_0$ the second step in the solution of the discretized problem (1) amounts to solving a second order elliptic boundary value problem discretized by means of finite elements. For this job no method can compete with the multigrid method in terms of efficiency [18, 30]. Multigrid is also a fast way to solve the discrete eddy current equations [33]. To apply a generic multigrid method we need several stacked finite element meshes and corresponding data structures.

A hierarchy of nested meshes also emerges naturally, when using modern *adaptive techniques*, which rely on local refinement [10, 12, 20, 48]: After the error of the discrete solution is estimated on a certain mesh, a new mesh is created by splitting elements into smaller ones where the accuracy is found wanting.

Multilevel data structures (cf. [9, 11, 39]) are challenging and take a big effort to implement. Nevertheless, the pay-off is substantial and multilevel approaches are gradually finding their way into engineering codes. We contend that one is well-advised to exploit available multiple levels of finite element meshes for the computation of the vector potential $\mathbf{H}_0$, too. In this paper I am going to present a computational procedure that is both cheap and nearly optimal in terms of the norm of the vector potential. A solid theoretical and algorithmic foundation will be laid.

The current work has its roots in the development of multilevel preconditioners for variational problems in the space $\boldsymbol{H}(\mathrm{div};\Omega)$. In this context, the multilevel computation of vector fields with a prescribed divergence has first been explored by Ewing and Wang [26] in 2D and was later generalized to 3D [34].

The plan of the paper is as follows: In the next section a few fundamental properties of the finite element spaces involved are summarized. The third section highlights the dangers of spanning tree techniques through some examples. The fourth section will give the details of the multilevel gauging algorithm. In the fifth section it will be established that the norm of the vector potential grows only linearly with number of mesh levels involved. In the following section the case of a perturbed discrete input current is examined. Finally, the norm of the multilevel gauging operator is studied numerically.

2. Finite Element Spaces

The computations are done on a polyhedral domain $\Omega \subset \mathbb{R}^3$. More generally, using so-called isoparametric finite elements [21, 23], domains with piecewise smooth boundary could be admitted, but we are not going to dwell on this point. The domain will be equipped with a triangulation $\mathscr{T}_h$ in the sense of [21] consisting of elements T. Those elements may be tetrahedra, hexahedra, prisms, or pyramids. The set of their faces will be denoted by $\mathscr{F}_h(\mathscr{T}_h)$, that of their edges by $\mathscr{E}_h(\mathscr{T}_h)$. Both, edges and faces are to be endowed with an inner orientation. Following [21], the shape regularity measure of a mesh $\mathscr{T}_h$ is defined as the maximum of the ratios of the diameter of the smallest circumscribed and the largest inscribed ball for every element.

A discrete 2-form on Ω w.r.t. $\mathscr{T}_h$ is represented by a $\boldsymbol{H}(\mathrm{div};\Omega)$-conforming finite element function built upon the mesh $\mathscr{T}_h$. The most prominent representatives of such finite elements are the Raviart–Thomas elements [41, 44], which have been constructed for all shapes of elements [19, 24, 28]. In the sequel, we confine ourselves to either hexahedral or tetrahedral meshes, but the extension of the algorithm to prisms and pyramids is pure routine.

We chose the symbol $\mathscr{RT}_k$ to designate the Raviart–Thomas space of polynomial order $k \in \mathbb{N}$. In the case of a tetrahedron T the local space is given by

$$\mathscr{RT}_k(T) := \{\mathbf{x} \mapsto \mathbf{p}_1(\mathbf{x}) + \mathbf{x} \cdot p_2(\mathbf{x}),\ \mathbf{p}_1 \in (\mathscr{P}_k(T))^3,\ p_2 \in \mathscr{P}_k(T),\ \mathbf{x} \in T\}.$$

Here, $\mathscr{P}_k(T)$ stands for the space of trivariate polynomials on T with total degree $\leq k$. A similar definition holds for a brick Q:

$$\mathscr{RT}_k(Q) := \mathscr{P}_{k+1,k,k}(Q) \times \mathscr{P}_{k,k+1,k}(Q) \times \mathscr{P}_{k,k,k+1}(Q),$$

where $\mathscr{P}_{k_1,k_2,k_3}(Q)$ is the space of polynomials of degree $\leq k_i$ in the variable x_i, $1 \leq i \leq 3$. Suitable degrees of freedoms (d.o.f.) for spaces of any polynomial order are available [19, 29, 32]. In the lowest order case they are given by the functionals of face fluxes expressed by

$$\kappa_F(\mathbf{v}) := \int_F \langle \mathbf{v}, \mathbf{n} \rangle d\sigma, \quad F \in \mathscr{F}_h(T).$$

This has earned the lowest order Raviart–Thomas elements the name *face elements*. For a tetrahedron with vertices $\mathbf{a}_1, \mathbf{a}_2, \mathbf{a}_3$, and $\mathbf{a}_4$ the corresponding four nodal basis functions read [17, Section 5.2.2]

$$\mathbf{b}_F^{(0)} := 2(\lambda_i \,\mathbf{grad}\, \lambda_j \times \mathbf{grad}\, \lambda_k + \lambda_j \,\mathbf{grad}\, \lambda_k \times \mathbf{grad}\, \lambda_i + \lambda_k \,\mathbf{grad}\, \lambda_i \times \mathbf{grad}\, \lambda_j),$$

with the λ_i, $i = 1, 2, 3, 4$, as the barycentric coordinate functions for vertex $\mathbf{a}_i$ and $F \in \mathscr{F}_h(T)$ spanned by the vertices $\mathbf{a}_i$, $\mathbf{a}_j$, and $\mathbf{a}_k$, $i < j < k$. Here, the orientation of F is implicitly provided by the order of its vertices.

For the second order space $\mathscr{RT}_1(T)$ additional degrees of freedom involve linear moments of normal components on faces and the integrals of each of the three components of the discrete vector field over the elements (cf. Fig. 1). As above, it is possible to specify the extra canonical basis functions for a tetrahedron T ($F \in \mathscr{F}(T)$):

$$\begin{aligned}
\mathbf{b}_{F,1}^{(1)} &:= 2\lambda_i \,\mathbf{grad}\, \lambda_j \times \mathbf{grad}\, \lambda_k - \lambda_j \,\mathbf{grad}\, \lambda_k \times \mathbf{grad}\, \lambda_i - \lambda_k \,\mathbf{grad}\, \lambda_i \times \mathbf{grad}\, \lambda_j \\
\mathbf{b}_{F,2}^{(1)} &:= 2\lambda_j \,\mathbf{grad}\, \lambda_i \times \mathbf{grad}\, \lambda_k - \lambda_i \,\mathbf{grad}\, \lambda_k \times \mathbf{grad}\, \lambda_j - \lambda_k \,\mathbf{grad}\, \lambda_j \times \mathbf{grad}\, \lambda_i \\
\mathbf{b}_{T,i}^{(1)} &:= \lambda_i \mathbf{b}_{F_i}^{(0)}, \quad i = 1, 2, 3.
\end{aligned}$$

As before, the face F is supposed to be spanned by the vertices $\mathbf{a}_i$, $\mathbf{a}_j$, and $\mathbf{a}_k$, $i < j < k$, and F_i denotes the face opposite to vertex $\mathbf{a}_i$. Note that the basis functions $\mathbf{b}_{F,1}^{(1)}$ and $\mathbf{b}_{F,2}^{(1)}$ are associated with (located at) the face F (When we state that a d.o.f./basis function is located at some geometric entity O, we have in mind that the d.o.f. can be expressed by an integral over O). The normal components of $\mathbf{b}_{T,i}^{(1)}$, $i = 1, 2, 3$, vanish on ∂T. As easily the basis functions for hexahedra can be specified. We remark that for a brick Q we have

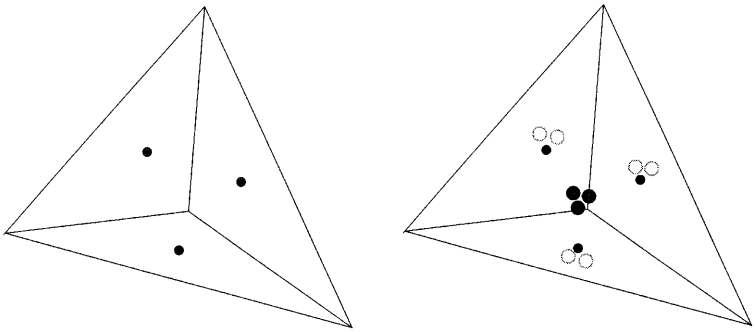

Figure 1. Location of degrees of freedom for lowest order (left) and first order (right) tetrahedral Raviart–Thomas elements: The filled disks stand for averages, the circles for linear moments of face fluxes. To avoid clutter the d.o.f. on the front face have been dropped

$\dim \mathscr{RT}_1(Q) = 36$, with four degrees of freedom associated with each face, and eight interior d.o.f.

The discrete vector potential to a discrete closed 1-form on $\mathscr{T}_h$ has to belong to a $\boldsymbol{H}(\mathbf{curl};\Omega)$-conforming finite element space on $\mathscr{T}_h$. Those are usually called Nédélec finite elements [41] and will be given the token $\mathscr{ND}$. Again, families of these elements are known for all shapes of elements [24, 28]. For a tetrahedron T the local spaces of polynomial order $k \in \mathbb{N}$ are given by

$$\mathscr{ND}_k(T) := \left\{ \mathbf{x} \mapsto \mathbf{p}_1(\mathbf{x}) + \mathbf{p}_2(\mathbf{x}), \quad \begin{array}{ll} \mathbf{p}_1 \in \mathscr{P}_{k-1}(T), & \mathbf{p}_2 \in \mathscr{P}_k(T), \\ \langle \mathbf{p}_2(\mathbf{x}), \mathbf{x} \rangle = 0 & \forall\, \mathbf{x} \in T \end{array} \right\},$$

whereas for a brick Q we have

$$\mathscr{ND}_k(Q) := \mathscr{P}_{k-1,k,k}(Q) \times \mathscr{P}_{k,k-1,k}(Q) \times \mathscr{P}_{k,k,k-1}(Q).$$

For the lowest order case, $k = 1$, the degrees of freedom are plain path integrals along the edges of the mesh ("edge voltages"), what accounts for the term *edge elements*. For a tetrahedral element T we find $\dim \mathscr{ND}_1(T) = 6$. The canonical basis function attached to the edge $E \in \mathscr{E}_h(T)$ linking vertices $\mathbf{a}_i$ and $\mathbf{a}_j$, $1 \le i < j \le 4$, turns out to be [17, Section 5.2.2,]

$$\beta_E^{(1)} := \lambda_i \, \mathbf{grad}\, \lambda_j - \lambda_j \, \mathbf{grad}\, \lambda_i.$$

Second order Nédélec elements on a tetrahedron feature two degrees of freedom per edge and another two d.o.f. for each face [41]. More precisely, those are the linear moments of the path integrals along edges and averages of

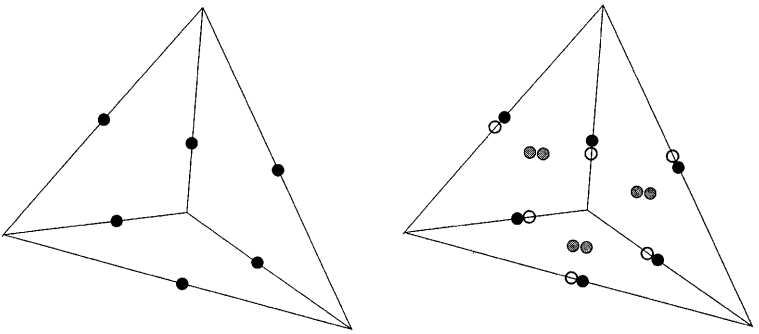

Figure 2. Location of degrees of freedom for lowest order (left) and first order (right) tetrahedral Nédélec elements: The filled disks stand for averages, the circles for linear moments of edge path integrals

tangential components over faces. The additional canonical basis functions read [45]

$$\beta_E^{(2)} := \lambda_i \,\mathbf{grad}\,\lambda_j + \lambda_j \,\mathbf{grad}\,\lambda_i, \quad E \in \mathscr{E}_h(T)$$

$$\beta_{F,1}^{(2)} := \lambda_i\lambda_j \,\mathbf{grad}\,\lambda_k - \lambda_i\lambda_k \,\mathbf{grad}\,\lambda_j, \quad F \in \mathscr{F}_h(T)$$

$$\beta_{F,2}^{(2)} := \lambda_j\lambda_i \,\mathbf{grad}\,\lambda_k - \lambda_j\lambda_k \,\mathbf{grad}\,\lambda_i, \quad F \in \mathscr{F}_h(T),$$

where the face F has vertices $\mathbf{a}_i$, $\mathbf{a}_j$, and $\mathbf{a}_k$, $1 \le i < j < k \le 4$.

For a brick, the path integrals along its 12 edges also supply the degrees of freedom for lowest order hexahedral Nédélec elements. In the second order case four more linear moments of the tangential components on each face and six linear moments in the interior of the element are required to determine the finite element function (see [41]).

Given the local representations and requiring that the degrees of freedom are meaningful on a global scale, we end up with the global finite element spaces $\mathscr{RT}_k(\Omega;\mathscr{T}_h)$ and $\mathscr{ND}_k(\Omega;\mathscr{T}_h)$. They have the desired normal and tangential continuity, what makes them subspaces of the Hilbert spaces $\boldsymbol{H}(\mathrm{div};\Omega)$ and $\boldsymbol{H}(\mathbf{curl};\Omega)$, respectively [41]. For a discussion of these function spaces see [27]. If the finite element functions are to belong to the corresponding spaces with homogeneous boundary conditions, we simply set d.o.f. on $\partial\Omega$ to zero. Such spaces will be labeled with subscript 0.

The local basis functions introduced above give rise to bases $\{\mathbf{b}_\kappa\}_\kappa$ and $\{\beta_\kappa\}_\kappa$ of $\mathscr{RT}_k(\Omega;\mathscr{T}_h)$ and $\mathscr{ND}_k(\Omega;\mathscr{T}_h)$, respectively. Here, the index κ runs through all global degrees of freedom. The basis functions are locally supported and form an L^2-*frame*. In other words, we can find generic constants $\underline{C}, \overline{C} > 0$, independent of the meshwidth h and only depending on k and the shape regularity measure of $\mathscr{T}_h$, such that

$$\begin{aligned}
\underline{C}\|\boldsymbol{\xi}_h\|^2_{\boldsymbol{L}^2(\Omega)} \leq \sum_{\kappa} \kappa(\boldsymbol{\xi}_h)^2 \|\boldsymbol{\psi}_\kappa\|^2_{\boldsymbol{L}^2(\Omega)} \leq \overline{C}\|\boldsymbol{\xi}_h\|^2_{\boldsymbol{L}^2(\Omega)} \quad \forall\, \boldsymbol{\xi}_h \in \mathscr{N}\mathscr{D}_k(\Omega;\mathscr{T}_h) \\
\underline{C}\|\mathbf{v}_h\|^2_{\boldsymbol{L}^2(\Omega)} \leq \sum_{\kappa} \kappa(\mathbf{v}_h)^2 \|\mathbf{j}_\kappa\|^2_{\boldsymbol{L}^2(\Omega)} \leq \overline{C}\|\mathbf{v}_h\|^2_{\boldsymbol{L}^2(\Omega)} \quad \forall\, \mathbf{v}_h \in \mathscr{R}\mathscr{T}_k(\Omega;\mathscr{T}_h).
\end{aligned} \tag{2}$$

This result can be obtained by a straightforward application of affine equivalence techniques [22, 23]. Following a popular convention, a capital C will indicate a generic constant. Its value can vary between different occurrences, but we will always specify what it must not depend on.

Throughout we are going to use the basis functions presented above. Then it makes sense to refer to the coefficient vector describing a finite element function. Those will be tagged by a small arrow on top of the symbol for a finite element function.

Our theory will make heavy use of the notion of *quasiuniformity*: The quasiuniformity measure of a mesh is the ratio of the greatest and smallest diameter of its elements. In the case of a small quasiuniformity measure the notion of a mesh-width h of $\mathscr{T}_h$ is sensible. As a special case of (2), quasiuniformity links Euclidean norms of coefficient vectors and the L^2-norms of finite element functions:

$$\begin{aligned}
|\vec{\mathbf{v}}_h|^2 &\approx h\|\mathbf{v}_h\|^2_{\boldsymbol{L}^2(\Omega)}, \quad \mathbf{v}_h \in \mathscr{R}\mathscr{T}_0(\Omega;\mathscr{T}_h) \\
|\vec{\boldsymbol{\xi}}_h|^2 &\approx h^{-1}\|\boldsymbol{\xi}\|^2_{\boldsymbol{L}^2(\Omega)}, \quad \boldsymbol{\xi}_h \in \mathscr{N}\mathscr{D}_1(\Omega;\mathscr{T}_h),
\end{aligned} \tag{3}$$

where $\approx$ stands for equivalence with constants only depending on the shape regularity and quasiuniformity measure of $\mathscr{T}_h$.

Given the degrees of freedom for the finite element spaces nodal interpolation operators $I_h : C(\Omega) \mapsto \mathscr{R}\mathscr{T}_0(\Omega;\mathscr{T}_h)$ and $\Pi_h : C(\Omega) \mapsto \mathscr{N}\mathscr{D}_1(\Omega;\mathscr{T}_h)$ can be defined (cf. [19]). Be aware that beyond continuous functions the interpolations operators remain well defined, for instance, for all conforming finite element functions on any mesh. The exceptional feature of the nodal interpolation operators is the *commuting diagram property* [26, 31]. It asserts that the diagram

$$\begin{array}{ccccc}
\boldsymbol{C}^\infty(\Omega) & \xrightarrow{\mathbf{curl}} & \boldsymbol{C}^\infty(\Omega) & \xrightarrow{\mathrm{div}} & C^\infty(\Omega) \\
\downarrow{\scriptstyle \Pi_h} & & \downarrow{\scriptstyle I_h} & & \downarrow{\scriptstyle Q_h} \\
\mathscr{N}\mathscr{D}_1(\Omega;\mathscr{T}_h) & \xrightarrow{\mathbf{curl}} & \mathscr{R}\mathscr{T}_0(\Omega;\mathscr{T}_h) & \xrightarrow{\mathrm{div}} & \mathscr{Q}_0(\Omega,\mathscr{T}_h)
\end{array} \tag{4}$$

commutes, where Q_h is the L^2-orthogonal projection onto the space $\mathscr{Q}_0(\Omega,\mathscr{T}_h)$ of piecewise constant, discontinuous functions on $\mathscr{T}_h$.

The commuting diagram property is the key to the proof of the following *representation theorem* [23, 32], which shows that essential algebraic properties of the function spaces are preserved in the discrete setting:

Theorem 1 (Discrete potentials). *Provided that* Ω *has no cavities we can conclude the existence of discrete vector potentials*:

$$\mathscr{RT}^0_k(\Omega;\mathscr{T}_h) := \{\mathbf{v}_h \in \mathscr{RT}_k(\Omega;\mathscr{T}_h),\ \operatorname{div}\mathbf{v}_h = 0\} = \mathbf{curl}\,\mathscr{ND}_{k+1}(\Omega;\mathscr{T}_h)$$

We add that the remarks made on the existence of a vector potentials in the introduction also carry over to the discrete setting, giving rise to discrete cohomology spaces [38].

3. Co-Tree Gauging

The gist of co-tree gauging is the selection of a subspace $\mathscr{ND}^+_1(\Omega;\mathscr{T}_h)$ of $\mathscr{ND}_1(\Omega;\mathscr{T}_h)$ such that $\mathbf{curl} : \mathscr{ND}^+_1(\Omega;\mathscr{T}_h) \mapsto \mathscr{RT}_0(\Omega;\mathscr{T}_h)$ is injective, i.e. $\mathscr{ND}^+_1(\Omega;\mathscr{T}_h)$ has to be an algebraic complement of the kernel of the **curl**-operator. This subspace is obtained as the span of a set of cunningly selected basis functions (see [17, Section 5.3], [23], and [37]) . These basis functions can be found by means of the previously mentioned spanning tree techniques:

For the sake of simplicity we assume a contractible domain Ω. We start by building a spanning tree τ of edges in $\mathscr{E}_h(\mathscr{T}_h)$, which is a maximal cycle-free subset of $\mathscr{E}_h(\mathscr{T}_h)$. Here a cycle is a closed curve formed by edges in $\mathscr{E}_h(\mathscr{T}_h)$. Algorithms are available that take $O(\sharp\mathscr{E}_h(\mathscr{T}_h))$ operations to determine the tree.

According to the definition of τ, for each edge E in the co-tree $\tau' := \mathscr{E}_h(\mathscr{T}_h)\backslash\tau$ we can find a cycle $\gamma_E \subset \mathscr{E}(\mathscr{T}_h)$ such that $\gamma_E \cap \tau = \gamma_E\backslash\{E\}$. Given $\mathbf{v}_h \in \mathscr{RT}^0_0(\Omega;\mathscr{T}_h)$ the construction of a vector potential $\boldsymbol{\xi}_h \in \mathscr{ND}_1(\Omega;\mathscr{T}_h)$ can be carried out as follows: For each $E \in \tau'$ let σ_E be some set of faces bounded by γ_E. Then

$$\boldsymbol{\xi}_h := \sum_{E\in\tau'}\left(\sum_{F\in\sigma_E} \pm\kappa_F(\mathbf{v}_h)\right)\cdot\beta_E \tag{5}$$

provides a vector potential for $\mathbf{v}_h$. The signs depend on the relative orientations of the individual faces w.r.t. the induced orientation of σ_E. Figure 3 depicts an example of a spanning tree of edges for a meshed cube.

The example from Fig. 3 discloses a fundamental drawback of cotree-gauging. By merely following the rules of the construction we may end up with a vector potential $\boldsymbol{\xi}_h$ whose L^2-norm is vastly greater than that of $\mathbf{v}_h$: Assume that an edge element function $\boldsymbol{\zeta}_h$ is given by prescribing value 1 for the d.o.f. at the locations of the bold arrows in Fig. 3. Now imagine that the same construction of $\boldsymbol{\zeta}_h$ and of the comb-like spanning tree is carried out for a regular hexahedral mesh with N elements in each coordinate direction, $N \in \mathbb{N}$. We examine the discrete vector potential $\boldsymbol{\xi}_h$ that co-tree gauging yields for the solenoidal face element vector field $\mathbf{v}_h := \mathbf{curl}\,\boldsymbol{\zeta}_h$. The degrees of freedom of $\boldsymbol{\xi}_h$ belonging to the z-edges (marked with delicate arrows) of the bottom layer of cubes can easily be calculated by counting the number of bold arrows contained in the related cycle. Hence, we get

$$|\vec{\boldsymbol{\xi}}_h|^2 \geq (N+1)\sum_{i=0}^{N}(2i+1)^2 = O(N^4) \text{ as } N\to\infty,$$

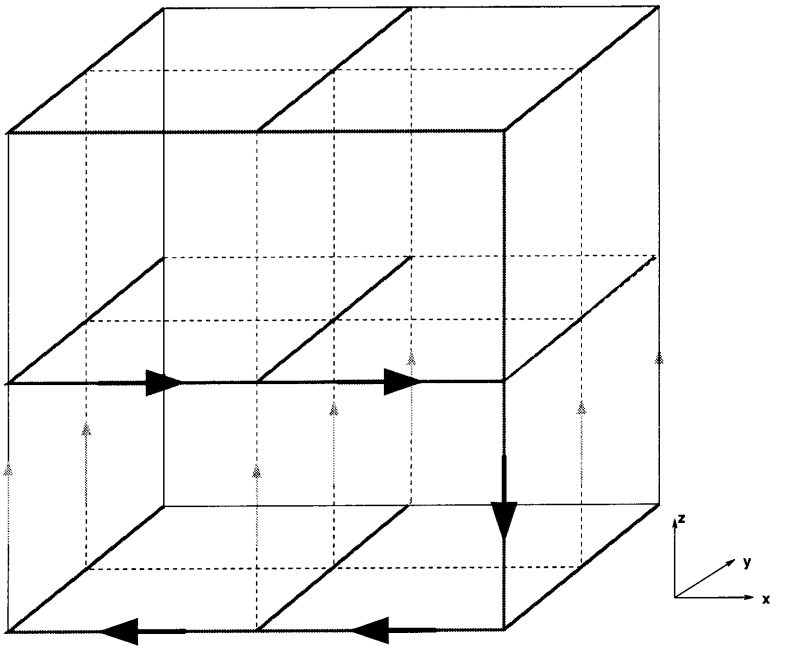

Figure 3. Example for cotree-gauging in three dimensions: Boldface edges indicate those belonging to the spanning tree

whereas

$$|\vec{\mathbf{v}}_h|^2 = 7N + 6.$$

Though the spanning tree employed in this example looks reasonable, by (3) we end up with an asymptotic estimate like ($h := N^{-1}$)

$$\|\boldsymbol{\xi}_h\|^2_{L^2(\Omega)} \approx h|\vec{\boldsymbol{\xi}}_h|^2 \approx h^{-2}|\vec{\mathbf{v}}_h|^2 \approx h^{-1}\|\mathbf{v}_h\|^2_{\boldsymbol{L}^2(\Omega)}, \tag{6}$$

where $\approx$ means equivalence up to small constants. On top of that, (6) is by no means the worst situation: More awkward spanning trees with $\|\boldsymbol{\xi}_h\|^2_{L^2(\Omega)} \approx h^{-2}\|\mathbf{v}_h\|^2_{\boldsymbol{L}^2(\Omega)}$ can easily be conceived.

4. Multilevel Gauging Procedure

Now, we consider a sequence of nested meshes $\mathscr{T}_0 \prec \mathscr{T}_1 \prec \cdots \prec \mathscr{T}_L$, $L \in \mathbb{N}$, that is, every element of $\mathscr{T}_k$ is the union of a small number of elements of the next finer mesh $\mathscr{T}_{k+1}$, $k = 0, \ldots, L-1$. We adopt the notations $\mathscr{F}_k := \mathscr{F}_f(\mathscr{T}_k)$, $\mathscr{E}_k := \mathscr{E}_h(\mathscr{T}_k)$ for the sets of faces and edges of $\mathscr{T}_k$, respectively.

Most commonly, such a sequence of meshes is generated by successive refinement of an initial triangulation $\mathscr{T}_0$. Several such refinement strategies are known, the

most commonplace being the so-called red-green refinement [13, 25] and bisection refinement [5, 8]. In the case of red-green refinement an element may be regularly refined by chopping it up into eight smaller elements of the same shape. Alternatively, to maintain conformity of the mesh, green refinement is employed. For a description we refer to [24]. The fundamental operation in bisection refinement of a tetrahedral mesh is a splitting of a tetrahedron into two by introducing a new vertex on a so-called refinement edge. What matters in the current context is that all schemes employ only a small number of refinement templates, sets of rules on how to split an element. On top of that, the refinement templates are affine invariant. In other words, application of a refinement template commutes with affine mappings.

All the refinement methods have been particularly designed to prevent severe deterioration of the shape regularity measure. Consequently, we can assume that all $\mathscr{T}_k$ sport the same shape regularity measure. We point out that the same element might be shared by several meshes in the case of local refinement.

For each element T except those contained in $\mathscr{T}_0$ we can find a unique "father" $\mathbf{T}_T \in \cup\mathscr{T}_k$ as the smallest element in which T is strictly contained. Thus, we can fix the level $l(T)$ of an element T through

$$l(T) = \begin{cases} 0 & \text{if } T \in \mathscr{T}_0 \\ l(\mathbf{T}_T) + 1 & \text{if } T \notin \mathscr{T}_0. \end{cases}$$

For the set of elements on a specific level we introduce the notation $\tilde{\mathscr{T}}_k := \{T \in \mathscr{T}_k, l(T) = k\}$. Evidently, in the case of local refinement we might encounter $\tilde{\mathscr{T}}_k \neq \mathscr{T}_k$. For convenience, we set $\hat{\mathscr{T}}_k := \{\mathbf{T} \in \tilde{\mathscr{T}}_k, \exists T \in \tilde{\mathscr{T}}_{k+1} : T \subset \mathbf{T}\}$. Analogously, the sets $\hat{\mathscr{E}}_k$ and $\hat{\mathscr{K}}_k$ contain those edges and faces on level k that have "children" on level $k+1$. We demand that the higher the level of an element T the smaller its diameter h_T: In quantitative terms, we require $h_T \approx \gamma^{l(T)}$ for some $0 < \gamma < 1$, where $\approx$ indicates a two-sided estimate with constants only depending on the shape regularity of $\mathscr{T}_0$. The refinement schemes mentioned above will meet these requirements.

We start with a solenoidal face element vector field $\mathbf{v}_h \in \mathscr{RT}_0^0(\Omega; \mathscr{T}_L)$, for which we seek a discrete vector potential $\boldsymbol{\xi}_h \in \mathscr{ND}_1(\Omega; \mathscr{T}_L)$, $\mathbf{curl}\, \boldsymbol{\xi}_h = \mathbf{v}_h$. We exploit the multilevel structure of the triangulations by performing a *hierarchic multilevel decomposition* of $\mathbf{v}_h$ (see [6, 7, 51] for more applications of hierarchical multilevel splittings in the finite element method):

$$\mathbf{v}_h = \sum_{k=0}^{L} \mathbf{v}_k, \quad \mathbf{v}_0 := I_0 \mathbf{v}_h \quad \text{and} \quad \mathbf{v}_k := (I_k - I_{k-1})\mathbf{v}_h, \quad k = 1, \ldots, L. \tag{7}$$

Here, we write $I_k : \mathscr{RT}_0(\Omega; \mathscr{T}_L) \mapsto \mathscr{RT}_0(\Omega; \mathscr{T}_k)$ for the nodal interpolation. Please keep in mind that the support of $\mathbf{v}_k$ is confined to the union of elements in $\tilde{\mathscr{T}}_k$, $k = 0, \ldots, L$. Furthermore, it is plain to see that the nodal values for the $\mathbf{v}_k$ can be computed cheaply and locally (see algorithm in Fig. 7).

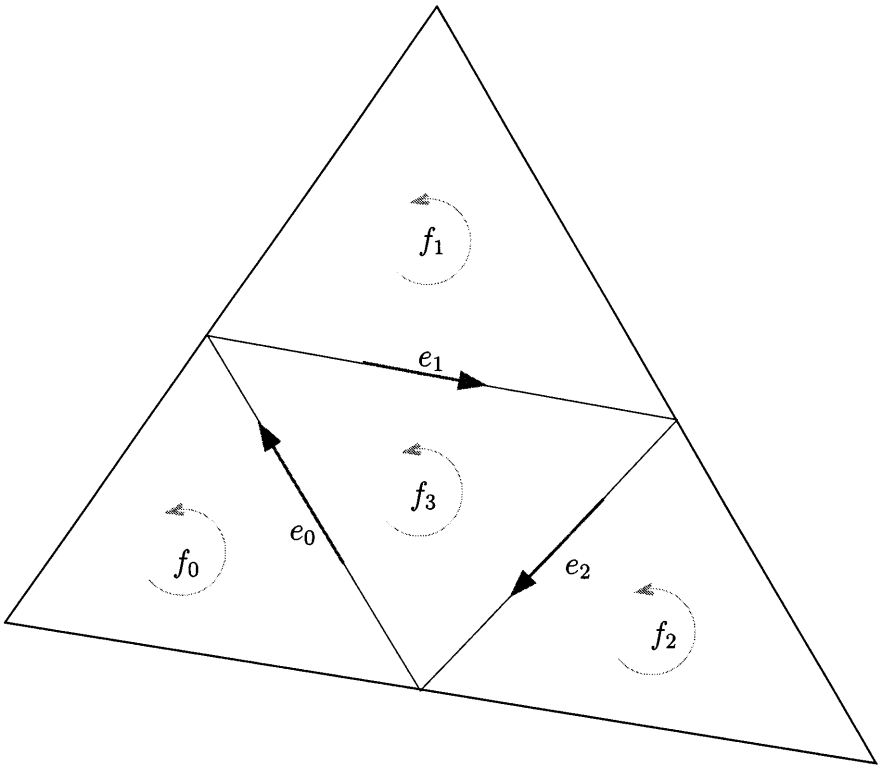

Figure 4. Regularly refined triangular face

As a consequence of the commuting diagram property (4), we note that the hierarchical surpluses $\mathbf{v}_k$ are solenoidal, i.e. $\operatorname{div} \mathbf{v}_k = 0$, $k = 0, \ldots, L$. Besides, from the very definition of the degrees of freedom in lowest order Raviart–Thomas spaces we learn that for $k \in \{1, \ldots, L\}$

$$\int_F \langle \mathbf{v}_k, \mathbf{n} \rangle d\sigma = 0 \quad \forall F \in \mathscr{F}_{k-1}. \tag{8}$$

Plainly speaking, the average of normal fluxes of hierarchical surpluses $\mathbf{v}_k$, $k = 1, \ldots, L$, through all faces of elements on coarser levels vanishes. Let us single out a face $F \in \hat{\mathscr{F}}_{k-1}$, $k = 1, \ldots, L$, that has been decomposed into four smaller face $f_0, f_1, f_2, f_3 \in \mathscr{F}_k$. If F is a triangle the resulting pattern of sub-triangles along with the internal orientations of faces and edges is sketched in Fig. 4.

Using the labels of Fig. 4, we denote by β_i, $i = 0, 1, 2$, the $\mathscr{N}\mathscr{D}_1$-basis function attached to edge e_i. By Stokes' theorem it satisfies

$$\int_{f_j} \langle \mathbf{curl}\, \beta_i, \mathbf{n} \rangle d\sigma = \delta_{i,j}, \quad i, j \in \{0, 1, 2\} \quad \text{and} \quad \int_{f_i \cup f_3} \langle \mathbf{curl}\, \beta_i, \mathbf{n} \rangle d\sigma = 0.$$

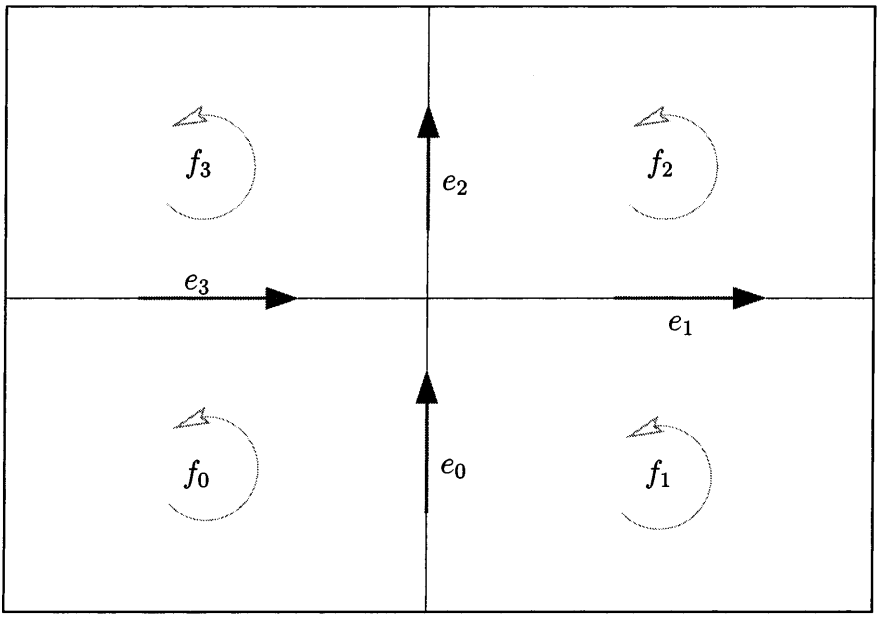

Figure 5. Regularly refined quadrilateral face

Now, we set

$$\boldsymbol{\eta}_F := \sum_{i=0}^{2} \left(\int_{f_i} \langle \mathbf{v}_k, \mathbf{n} \rangle d\sigma \right) \cdot \beta_i. \tag{9}$$

Taking into account that the normal components of $\mathbf{v}_k$ are constant on faces of $\mathscr{T}_k$, a straightforward computation yields $\langle \mathbf{curl}\, \boldsymbol{\eta}_F, \mathbf{n} \rangle_{|f_i} = \langle \mathbf{v}_k, \mathbf{n} \rangle_{|f_i}$, $i = 0, 1, 2$. In combination with (8) this means:

$$\langle \mathbf{curl}\, \boldsymbol{\eta}_F, \mathbf{n} \rangle_{|F} = \langle \mathbf{v}_k, \mathbf{n} \rangle_{|F}. \tag{10}$$

Besides complete subdivision, F could also have been cut into two halves by one new edge. To determine a suitable $\boldsymbol{\eta}_F$ is all but trivial then. We omit the details.

In the case of a quadrilateral $F \in \hat{\mathscr{F}}_{k-1}$, the procedure is similar (see Fig. 5). Setting $\phi_i := \int_{f_i} \langle \mathbf{v}_k, \mathbf{n} \rangle d\sigma$ and $\epsilon_i := \int_{e_i} \langle \mathbf{v}_k, \mathbf{t} \rangle d\Gamma$, $i = 0, 1, 2, 3$, Stokes' theorem implies

$$\begin{pmatrix} 1 & 0 & 0 & -1 \\ -1 & -1 & 0 & 0 \\ 0 & 1 & -1 & 0 \\ 0 & 0 & 1 & -1 \end{pmatrix} \begin{pmatrix} \epsilon_0 \\ \epsilon_1 \\ \epsilon_2 \\ \epsilon_3 \end{pmatrix} = \begin{pmatrix} \phi_0 \\ \phi_1 \\ \phi_2 \\ \phi_3 \end{pmatrix} \tag{11}$$

By (8) we know $\phi_0 + \phi_1 + \phi_2 + \phi_3 = 0$ so that (11) becomes solvable. Recalling the objective to find a vector potential with small norm, we should use the Moore–Penrose pseudo inverse to determine a solution of (11) of minimal Euclidean norm:

$$\begin{pmatrix} \epsilon_0 \\ \epsilon_1 \\ \epsilon_2 \\ \epsilon_3 \end{pmatrix} = \frac{1}{2} \begin{pmatrix} 1 & -1 & -1 & -1 \\ -1 & -1 & 1 & 1 \\ -1 & -1 & -1 & 1 \\ -1 & -1 & -1 & -1 \end{pmatrix} \begin{pmatrix} \phi_0 \\ \phi_1 \\ \phi_2 \\ \phi_3 \end{pmatrix} \tag{12}$$

By plain computation we can verify that $\boldsymbol{\eta}_F := \sum_{i=0}^{3} \epsilon_i \beta_i$, $\beta_i := \beta_{e_i}$, satisfies (10).

Owing to its construction $\mathbf{curl}\, \boldsymbol{\eta}_F$ has vanishing normal components on any other face of $\mathscr{F}_{k-1}$ except F. Therefore summing up all $\boldsymbol{\eta}_F$, $F \in \hat{\mathscr{F}}_{k-1}$, results in a vector field called $\boldsymbol{\eta}_k \in \mathscr{NP}_1(\Omega; \mathscr{T}_k)$ that features property (10) for every face $F \in \mathscr{F}_{k-1}$. The remainder $\tilde{\mathbf{v}}_k := \mathbf{v}_k - \mathbf{curl}\, \boldsymbol{\eta}_k$ is a vector field in $\mathscr{RT}^0_0(\Omega; \mathscr{T}_k)$ which consists of isolated components confined to the interior of elements of $\hat{\mathscr{T}}_{k-1}$, i.e.

$$\tilde{\mathbf{v}}_k \in \bigotimes_{\mathbf{T} \in \hat{\mathscr{T}}_{k-1}} \mathscr{RT}^0_{0,0}(\mathbf{T}; \mathscr{T}_{k|\mathbf{T}}).$$

Then we can apply Theorem 1 locally to each $\mathbf{T} \in \mathscr{T}_{k-1}$. It guarantees the existence of an $\mathscr{NP}_1$-vector field $\boldsymbol{\eta}'_{k,\mathbf{T}}$, supported on $\mathbf{T}$, whose **curl** agrees with $\tilde{\mathbf{v}}_{k|\mathbf{T}}$. Let us take a closer look at the construction for a regularly (“red”) refined tetrahedron that possesses one new interior edge as in Fig. 6.

Using the labels of Fig. 6, we see that there are four $f_i := [\mathbf{p}, \mathbf{q}, m_i]$, $i = 1, \ldots, 4$, adjacent to the interior edge $[\mathbf{p}, \mathbf{q}]$. Setting $\phi_i := \int_{f_i} \langle \tilde{\mathbf{v}}_k, \mathbf{n} \rangle d\sigma$ we may choose (with signs depending on orientation)

$$\boldsymbol{\eta}'_{k,\mathbf{T}} := \tfrac{1}{4}(\pm\phi_1 \pm \phi_2 \pm \phi_3 \pm \phi_4) \cdot \beta_{[\mathbf{p},\mathbf{q}]}, \tag{13}$$

and one quickly verifies $\mathbf{curl}\, \boldsymbol{\eta}'_{k,\mathbf{T}} = \tilde{\mathbf{v}}_k$ on $\mathbf{T}$. The fluxes ϕ_i are readily available, for instance (see Fig. 6)

$$\phi_3 = \kappa_{f_3}(\mathbf{v}_k) - \kappa_e(\boldsymbol{\eta}_k) - \kappa_{e'}(\boldsymbol{\eta}_k).$$

For most other meaningful refinement templates for a tetrahedron, e.g. those underlying the green refinements, no new internal edges are created and this step of the procedure can be skipped.

For a hexahedral mesh the procedure is almost the same. Yet, when fixing the edge voltages for the six interior edges of a regularly refined brick, we again encounter non-uniqueness. As in the case of a quadrilateral face (12), a pseudo-inverse will deal with it.

The bottom line is that by adding up the local stream functions $\boldsymbol{\eta}'_{k,\mathbf{T}}$ over all macro-elements $\mathbf{T} \in \widehat{\mathscr{T}}_{k-1}$ we obtain a vector field

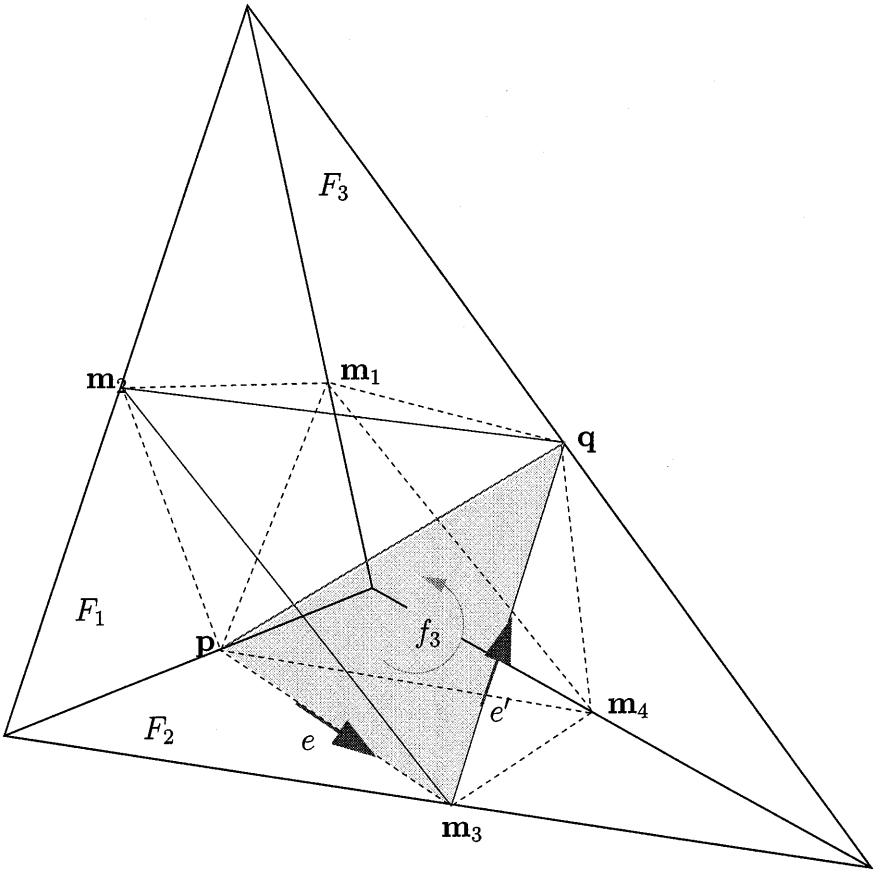

Figure 6. Regularly refined tetrahedron $\mathbf{T}$ with one internal edge for which a d.o.f. of the vector potential has to be determined

$$\boldsymbol{\xi}_k := \boldsymbol{\eta}_k + \sum_{\mathbf{T}\in\hat{\mathscr{T}}_{k-1}} \boldsymbol{\eta}'_{k,\mathbf{T}} \in \mathscr{ND}_1(\Omega;\mathscr{T}_k) \tag{14}$$

such that $\mathbf{curl}\,\boldsymbol{\xi}_k = \mathbf{v}_k$. On top of that, the d.o.f. of $\boldsymbol{\xi}_k$ that are located in $\mathbf{T} \in \hat{\mathscr{T}}_{k-1}$ can be computed from the d.o.f. of $\mathbf{v}_k$ in $\mathbf{T}$ by a simple linear mapping. Most important, thanks to affine invariance of the refinement algorithm, this mapping only depends on the refinement template applied to $\mathbf{T}$ and not on its actual shape. Thus, there is only a fixed small number of different mappings, which can be determined in advance.

On the coarsest mesh $\mathscr{T}_0$ we have to resort to a global computation of a discrete vector potential $\boldsymbol{\xi}_0 \in \mathscr{ND}_1(\Omega;\mathscr{T}_0)$ for $\mathbf{v}_0 \in \mathscr{RT}_0^0(\Omega;\mathscr{T}_0)$. We may rely on co-tree gauging now, since its inherent instability is offset by the small number of elements in $\mathscr{T}_0$. In order to play safe, we can also tackle the following saddle point problem [43] directly:

Seek $(\boldsymbol{\xi}_0, \mathbf{j}_0, p_0) \in \mathscr{ND}_1(\Omega; \mathscr{T}_0) \times \mathscr{RT}_0(\Omega; \mathscr{T}_0) \times \mathscr{Q}_0(\Omega, \mathscr{T}_0)$ such that

$$\begin{aligned}(\boldsymbol{\xi}_0, \boldsymbol{\eta}_0)_{\boldsymbol{L}^2(\Omega)} + (\mathbf{curl}\, \boldsymbol{\eta}_0, \mathbf{j}_0)_{\boldsymbol{L}^2(\Omega)} &= 0\\ (\mathbf{curl}\, \boldsymbol{\xi}_0, \mathbf{q}_0)_{\boldsymbol{L}^2(\Omega)} + (\operatorname{div} \mathbf{q}_0, p_0)_{\boldsymbol{L}^2(\Omega)} &= (\mathbf{v}_0, \mathbf{q}_0)_{\boldsymbol{L}^2(\Omega)}\\ (\operatorname{div} \mathbf{j}_0, w)_{L^2(\Omega)} &= 0 \end{aligned} \tag{15}$$

for all $\boldsymbol{\eta}_0 \in \mathscr{ND}_1(\Omega; \mathscr{T}_0)$, $\mathbf{q}_0 \in \mathscr{RT}_0(\Omega; \mathscr{T}_0)$, and $w \in \mathscr{Q}_0(\Omega, \mathscr{T}_0)$. Then, $\|\boldsymbol{\xi}_0\|_{\boldsymbol{L}^2(\Omega)} \leq C\|\mathbf{v}_0\|_{\boldsymbol{L}^2(\Omega)}$, with $C > 0$ depending on Ω only, is guaranteed and for coarse meshes of moderate size the computational effort is acceptable. We point out that the L^2-inner product in (15) can be replaced by plain Euclidean inner products of the vectors of d.o.f. This forfeits unconditional stability of $\boldsymbol{\xi}_0$, but greatly facilitates the solution of (15).

Ultimately, summing up the $\boldsymbol{\xi}_k$, $k = 0, \ldots, L$, we get the desired discrete vector potential $\boldsymbol{\xi}_h := \sum_{k=0}^{L} \boldsymbol{\xi}_k$. The corresponding computational procedure amounts to successively prolongating nodal values from coarse grid edges to those of the fine grid. These are local transfer operators, whose weights can be determined from the imbedding $\mathscr{ND}_1(\Omega; \mathscr{T}_{k-1}) \subset \mathscr{ND}_1(\Omega; \mathscr{T}_k)$ [33].

The complete algorithm is outlined in Fig. 7. There $\mathscr{RT}_0^0$ and $\mathscr{ND}_1$ have to be read as data-types handling the degrees of freedom of the finite element functions on all levels of refinement. The notation $\kappa(\mathbf{x}, O)$ symbolizes the access to that nodal value of the finite element function $\mathbf{x}$ located at the geometric object O. Again, we point out that all weights in the sums are affine invariant. Eventually, $\prec$ indicates the "father–son" relationship for geometric objects in the context of refinement.

A closer scrutiny reveals that due to the geometric decrease of the number of elements in "ancestral generations"

$$\sum_{k=0}^{L} \sharp\tilde{\mathscr{T}}_k \leq 2\sharp\mathscr{T}_L.$$

As a consequence, the total number of operations to compute $\boldsymbol{\xi}_h$ by the multilevel gauging algorithm of Fig. 7 is a small multiple of the number of elements of the finest mesh $\mathscr{T}_L$ (c.f. "local multigrid" [40]). In short, the algorithm has optimal complexity.

Remark. In case of a non-existent vector potential (as discussed in the introduction) the stage where the algorithm might run into difficulties is the calculation of the vector potential on the coarsest mesh $\mathscr{T}_0$. Then we have to resign to finding a $\boldsymbol{\xi}_0$ such that

$$\mathbf{v}_0 = \mathbf{curl}\, \boldsymbol{\xi}_0 + \mathbf{h}_0,$$

gauge(int k, $\mathcal{RT}_0^0$ &$\mathbf{v}$, $\mathcal{ND}_1$&$\boldsymbol{\xi}$)
{
if $(k > 0)$ {
// Compute hierarchical surpluses and d.o.f. of $\boldsymbol{\xi}_k$.
forall $(F \in \widehat{\mathcal{F}}_{k-1})$ {
$\kappa(\mathbf{v}, F) =$ sum of $\pm\kappa(\mathbf{v}, f)$, $f \prec F$.
forall $(f \prec F)$ { $\kappa(\mathbf{v}, f)$ -= weight $\cdot \pm\kappa(\mathbf{v}, F)$; }
forall $(e \in \{e' \in \mathcal{E}_k,\ e' \subset F)$
Set the degrees of freedom $\kappa(\boldsymbol{\xi}, e)$ of $\boldsymbol{\eta}_F$ according to (9) or (12).
}
forall $(\mathbf{T} \in \widehat{\mathcal{T}}_{k-1})$ {
forall $(f \in \{f' \in \mathcal{F}_k,\ f'$ is in the interior of $\mathbf{T}\})$ {
Set $\kappa(\mathbf{v}, f)$ as the nodal value of the hierarchical surplus $\mathbf{v}_k$. This can be done by adding a weighted sum of the values $\kappa(\mathbf{v}, F)$, $F \in \mathcal{F}_{k-1}$, $F \subset \partial\mathbf{T}$, to $\kappa(\mathbf{v}, f)$.
}
forall $(e \in \{e' \in \mathcal{E}_k,\ e'$ is in the interior of $\mathbf{T}\})$
Set $\kappa(\boldsymbol{\xi}, e)$ as the degree of freedom of $\boldsymbol{\eta}'_{k,\mathbf{T}}$ according to (13).
}
// Recursive call
gauge(k-1,**v**,$\boldsymbol{\xi}$);
// Compute prolongation of vector potential on next coarser level and add it to
// $\boldsymbol{\xi}_k$ *in order to determine vector potential for* $I_k\mathbf{v}_h$.
forall $(E \in \widehat{\mathcal{E}}_{k-1})$ {
forall $(e \prec E)$ { $\kappa(e, \boldsymbol{\xi})$ -= $\pm\frac{1}{2}\kappa(E, \boldsymbol{\xi})$; }
forall $(F \in \widehat{\mathcal{F}}_{k-1})$ {
forall $(e \in \{e' \in \mathcal{E}_k,\ e'$ is in the interior of $F\})$
Add to $\kappa(e, \boldsymbol{\xi})$ a weighted sum of $\kappa(E, \boldsymbol{\xi})$, $E \in \mathcal{E}_k$, $E \subset \partial F$.
}
forall $(\mathbf{T} \in \widehat{\mathcal{T}}_{k-1})$ {
forall $(e \in \{e' \in \mathcal{E}_k,\ e'$ is in the interior of $\mathbf{T}\})$
Add to $\kappa(e, \boldsymbol{\xi})$ a weighted sum of $\kappa(E, \boldsymbol{\xi})$, $E \in \mathcal{E}_k$, E is edge of $\mathbf{T}$.
}
}
}
else {
Solve the saddle point problem (15) on the coarsest mesh $\mathcal{T}_0$ in order to determine the degrees of freedom for $\boldsymbol{\xi}_0$ on $\mathcal{T}_0$.
}
}

Figure 7. Algorithm for multilevel gauging for lowest order elements

where $\mathbf{h}_0$ belongs to a discrete cohomology space $\mathscr{H}_2$ for $\mathscr{T}_0$. Such a $\mathbf{h}_0$ can be found using the "belted tree approach" described in [37]. As $\mathscr{T}_0$ consists of merely a few elements, neither the effort to determine $\mathbf{h}_0$ is prohibitive nor its norm is distressingly large. In sum, multilevel gauging does a good job also in this case.

So far, we have treated only the lowest order elements. We will not deal with the most general case, but argue that discussing the second order case sufficiently reveals the policy. Let us first take a look at tetrahedral meshes and consider $\mathscr{RT}^0_1(\Omega;\mathscr{T}_L)$. For any $T \in \mathscr{T}_L$ the divergences of the three nodal basis functions $\mathbf{b}^{(1)}_{T,i}$, $i = 1,2,3$, have vanishing mean value and are linearly independent. We conclude that if $\operatorname{div}\mathbf{v}_h = 0$, then these basis functions cannot make a contribution to $\mathbf{v}_h$. To get rid of the remaining higher order parts, we point out that $\mathbf{curl}\,\beta^{(2)}_{F,i} = \mathbf{b}^{(1)}_{F,i}$, $i = 1,2$ holds for each $F \in \mathscr{F}_L$ [42]. This permits us to calculate the vector potential $\boldsymbol{\xi}_h$ for

$$\mathbf{v}_h = \mathbf{v}_h^{(0)} + \mathbf{v}_h^{(1)}, \quad \mathbf{v}_h^{(1)} := \sum_{F\in\mathscr{F}_L} \alpha_{F,1}\mathbf{b}^{(1)}_{F,1} + \alpha_{F,2}\mathbf{b}^{(1)}_{F,2} \in \mathscr{RT}^0_1(\Omega;\mathscr{T}_L),\ \alpha_{F,i} \in \mathbb{R}, \quad (16)$$

as

$$\boldsymbol{\xi}_h = \boldsymbol{\xi}_h^{(0)} + \boldsymbol{\xi}_h^{(1)}, \quad \boldsymbol{\xi}_h^{(1)} := \sum_{F\in\mathscr{F}_L} \alpha_{F,1}\beta^{(2)}_{F,1} + \alpha_{F,2}\beta^{(2)}_{F,2}, \quad (17)$$

where $\boldsymbol{\xi}_h^{(0)}$ is the vector potential for $\mathbf{v}_h^{(0)} \in \mathscr{RT}^0_0(\Omega;\mathscr{T}_L)$ obtained through multilevel gauging. A similar reasoning applies to hexahedral meshes. In this case the higher order $\mathscr{ND}_2$-basis functions located at faces or within the element provide potentials for the higher order components of $\mathbf{v}_h \in \mathscr{ND}_2(\Omega;\mathscr{T}_L)$ at the same locations.

Remark. Note that the hierarchic decomposition automatically respects homogeneous boundary values. Hence, the multilevel gauging will yield a vector potential $\boldsymbol{\xi}_h$ with $\boldsymbol{\xi}_h \times \mathbf{n} = 0$ on Γ_D, if $\langle \mathbf{v}_h, \mathbf{n}\rangle = 0$ there and such a vector potential can be computed on $\mathscr{T}_0$.

5. Stability

By the open mapping theorem we see that with a constant depending on Ω only

$$\inf\{\|\boldsymbol{\xi}\|_{\boldsymbol{L}^2(\Omega)},\ \boldsymbol{\xi} \in \boldsymbol{H}(\mathbf{curl};\Omega),\ \mathbf{curl}\,\boldsymbol{\xi} = \mathbf{v}\} \geq C\|\mathbf{v}\|_{L^2(\Omega)} \quad \forall\,\mathbf{v} \in \mathbf{H}^0(\operatorname{div};\Omega).$$

On the other hand, from [3, Proposition 4.6] we learn that for all $\mathbf{v}_h \in \mathscr{RT}^0_0(\Omega;\mathscr{T}_h)$

$$\inf\{\|\boldsymbol{\xi}_h\|_{\boldsymbol{L}^2(\Omega)},\ \boldsymbol{\xi}_h \in \mathscr{ND}_1(\Omega;\mathscr{T}_h),\ \mathbf{curl}\,\boldsymbol{\xi}_h = \mathbf{v}_h\} \leq C\|\mathbf{v}_h\|_{\boldsymbol{L}^2(\Omega)},$$

where only Ω and the shape regularity measure of $\mathscr{T}_h$ enter the constant. Thus, the best we can hope for is to find a vector potential whose L^2-norm is uniformly bounded by that of $\mathbf{v}_h$. As we saw in Section 3, co-tree gauging falls way short of meeting this goal. The situation with multilevel gauging will be examined now:

Lemma 1. *Assume $\mathscr{T}_k$, $0 \le k \le L$, to be uniformly shape regular and quasi-uniform with meshwidth h_k. For $0 \le l < k \le L$, let E be an edge on level l and denote by $\omega_{E,k}$ the union of those elements of $\mathscr{T}_k$ for which one edge is contained in E. Accordingly, for a face $F \in \mathscr{F}_l$ the domain $\omega_{F,k}$ will be defined. Then there are constants $C > 0$, depending only on shape regularity and quasiuniformity measure of the meshes, such that*

$$(i)\ |\kappa_E(\boldsymbol{\mu}_k)|^2 \le Ch_l h_k^{-2} \|\boldsymbol{\mu}_k\|^2_{\boldsymbol{L}^2(\Omega_E)}, \quad \forall\, \boldsymbol{\mu}_k \in \mathscr{N}\mathscr{D}_1(\Omega;\mathscr{T}_k).$$
$$(ii)\ |\kappa_F(\mathbf{q}_k)|^2 \le Ch_l^2 h_k^{-1} \|\mathbf{q}_k\|^2_{\boldsymbol{L}^2(\Omega_F)}, \quad \forall\, \mathbf{q}_k \in \mathscr{R}\mathscr{T}_0(\Omega;\mathscr{T}_k).$$

Proof: Ad (i): By the L^2-stability of the nodal basis from (3) we can estimate

$$\begin{aligned}\kappa_E(\boldsymbol{\mu}_k)^2 &= \left(\sum_{e\subset E, e\in\mathscr{E}_k} \kappa_e(\boldsymbol{\mu}_k)\right)^2 \le \sharp\{e\in\mathscr{E}_k, e\subset E\}\cdot \sum_{e\subset E, e\in\mathscr{E}_k} \kappa_e(\boldsymbol{\mu}_k)^2 \\ &\le Ch_k^{-1}\sharp\{e\in\mathscr{E}_k, e\subset E\}\cdot \|\boldsymbol{\mu}_k\|^2_{\boldsymbol{L}^2(\omega_{E,k})}.\end{aligned}$$

Thanks to shape regularity $\sharp\{e\in\mathscr{E}_k, e\subset E\} \le Ch_l/h_k$ and we are done with (i). We skip the similar proof of (ii). □

Uniform shape regularity of the sequence of meshes guarantees that there is a small bound on the number of overlapping $\omega_{E,k}$. This makes

$$\sum_{E\in\mathscr{E}_l} \|\boldsymbol{\mu}_k\|^2_{\boldsymbol{L}^2(\omega_{E,k})} \le C\|\boldsymbol{\mu}_k\|^2_{\boldsymbol{L}^2(\Omega)} \tag{18}$$

hold, $C > 0$ depending on shape regularity.

The following theorem is a fundamental result about the multilevel decomposition of $\boldsymbol{H}(\mathrm{div};\Omega)$-conforming finite element spaces:

Theorem 2 (Multilevel decomposition of face element spaces). *Assume that Ω is a convex polyhedron and that the nested meshes $\mathscr{T}_k$, $0 \le k \le L$, are uniformly shape regular and quasi-uniform with geometrically decreasing meshwidths h_k. Then for each $\mathbf{v}_h$ in $\mathscr{R}\mathscr{T}_0(\Omega;\mathscr{T}_L)$ we can find decompositions*

$$\mathbf{v}_h = \mathbf{curl}\,\boldsymbol{\mu}_h + \mathbf{q}_h, \quad \boldsymbol{\mu}_h \in \mathscr{N}\mathscr{D}_1(\Omega;\mathscr{T}_L), \quad \mathbf{q}_h \in \mathscr{R}\mathscr{T}_0(\Omega;\mathscr{T}_L),$$

$$\boldsymbol{\mu}_h = \sum_{k=0}^{L} \boldsymbol{\mu}_k, \quad \boldsymbol{\mu}_k \in \mathscr{N}\mathscr{D}_1(\Omega;\mathscr{T}_k), \quad \textit{and} \quad \mathbf{q}_h = \sum_{k=0}^{L} \mathbf{q}_k, \quad \mathbf{q}_k \in \mathscr{R}\mathscr{T}_0(\Omega;\mathscr{T}_k),$$

such that

$$\|\mathbf{q}\|_{\boldsymbol{L}^2(\Omega)} \leq C\|\operatorname{div}\mathbf{v}_h\|_{L^2(\Omega)},$$

$$\|\mathbf{curl}\,\boldsymbol{\mu}_0\|^2_{L^2(\Omega)}+\sum_{k=1}^{L} h_k^{-2}\|\boldsymbol{\mu}_k\|^2_{\boldsymbol{L}^2(\Omega)} \leq C\|\mathbf{curl}\,\boldsymbol{\mu}_h\|^2_{\boldsymbol{L}^2(\Omega)},$$

$$\|\mathbf{q}_0\|^2_{\boldsymbol{H}(\operatorname{div};\Omega)}+\sum_{k=1}^{L} h_k^{-2}\|\mathbf{q}_k\|^2_{\boldsymbol{L}^2(\Omega)} \leq C\|\mathbf{q}_h\|^2_{\boldsymbol{H}(\operatorname{div};\Omega)},$$

where the constants depend on Ω *and the shape regularity and quasiuniformity measure of the meshes only.*

Proof: For the proof we refer to [31, 35]. It can also be inferred from the results in [4] (Proposition 4.3). □

Theorem 3. *For all* $\mathbf{v}_h \in \mathscr{RT}^0_0(\Omega;\mathscr{T}_L)$ *holds*

$$\|I_0\mathbf{v}_h\|^2_{\boldsymbol{L}^2(\Omega)}+\sum_{k=1}^{L}\|(I_k - I_{k-1})\mathbf{v}_h\|^2_{\boldsymbol{L}^2(\Omega)} \leq CL^2\|\mathbf{v}_h\|^2_{\boldsymbol{L}^2(\Omega)},$$

with a constant $C > 0$ *only depending of the shape regularity of the meshes.*

Proof: To begin with, assume that refinement has been uniform resulting in a quasi-uniform family of meshes $\{\mathscr{T}_k\}_{k=0}^{L}$. As the assertion is invariant w.r.t. simple scaling, we can set $h_0 := 1$ without loss of generality. Then pick a single (convex!) element D of $\mathscr{T}_0$. Applying Theorem 2 to $\mathbf{v}_h \in \mathscr{RT}^0_0(D;\mathscr{T}_L)$ shows the existence of $\boldsymbol{\mu}_k \in \mathscr{ND}_1(D;\mathscr{T}_k)$ such that ($\boldsymbol{\mu}_h := \sum_{k=0}^{L}\boldsymbol{\mu}_k$)

$$\mathbf{curl}\,(\boldsymbol{\mu}_h) = \mathbf{v}_h \quad \text{and} \quad \|\mathbf{curl}\,\boldsymbol{\mu}_0\|^2_{\boldsymbol{L}^2(D)} + \sum_{k=1}^{L} h_k^{-2}\|\boldsymbol{\mu}_k\|^2_{\boldsymbol{L}^2(D)} \leq \|\mathbf{v}_h\|^2_{\boldsymbol{L}^2(D)}.$$

Observing that $\boldsymbol{\mu}_k \in \mathscr{ND}_1(D;\mathscr{T}_k)$ we arrive at

$$(\Pi_l - \Pi_{l-1})\boldsymbol{\mu}_h = \boldsymbol{\mu}_l + \underbrace{\Pi_l\left(\sum_{k=l+1}^{L}\boldsymbol{\mu}_k\right)}_{=:\tilde{\boldsymbol{\mu}}_l} - \underbrace{\Pi_l\left(\sum_{k=l}^{L}\boldsymbol{\mu}_k\right)}_{=:\tilde{\boldsymbol{\mu}}_{l-1}}. \tag{19}$$

The following estimate first relies on the L^2-stability of the bases according to (3)

$$\sum_{l=0}^{L-1} h_l^{-2}\|\tilde{\boldsymbol{\mu}}_l\|^2_{\boldsymbol{L}^2(D)} \leq \sum_{l=0}^{L-1} h_l^{-1}\sum_{E\in\mathscr{E}_l^D}\kappa_E(\tilde{\boldsymbol{\mu}}_l)^2 = C\sum_{l=0}^{L-1} h_l^{-1}\sum_{E\in\mathscr{E}_l}\left(\sum_{k=l+1}^{L}\kappa_E(\boldsymbol{\mu}_k)\right)^2$$

then uses the Cauchy–Schwarz inequality and Lemma 1, part (i)

$$\leq C \sum_{l=0}^{L-1} h_l^{-1} \sum_{E \in \mathscr{E}_l^D} (L-l-1) \sum_{k=l+1}^{L} h_l h_k^{-2} \|\boldsymbol{\mu}_k\|^2_{\boldsymbol{L}^2(\omega_{E,k})}$$

and the equivalence (18).

$$\leq C \sum_{l=0}^{L-1} \sum_{k=l+1}^{L} h_k^{-2} (L-l-1) \|\boldsymbol{\mu}_k\|^2_{\boldsymbol{L}^2(D)}$$

Finally, the geometric decrease of the meshwidths and Theorem 2 are put to use:

$$\sum_{l=0}^{L-1} h_l^{-2} \|\tilde{\boldsymbol{\mu}}_l\|^2_{\boldsymbol{L}^2(D)} \leq CL^2 \sum_{k=1}^{L} h_k^{-2} \|\boldsymbol{\mu}_k\|^2_{\boldsymbol{L}^2(D)} \leq CL^2 \|\mathbf{v}_h\|^2_{\boldsymbol{L}^2(D)}$$

By the commuting diagram property (4) and (19), in connection with an inverse inequality for edge elements

$$\|\mathbf{curl}\, \boldsymbol{\eta}_k\|_{\boldsymbol{L}^2(D)} \leq Ch_k^{-1} \|\boldsymbol{\eta}_k\|_{\boldsymbol{L}^2(D)}, \quad \forall \eta_k \in \mathscr{NED}_1(\Omega; \mathscr{T}_k),$$

we see

$$\begin{aligned}
\sum_{l=1}^{L} \|(I_l - I_{l-1})\mathbf{v}_h\|^2_{\boldsymbol{L}^2(D)} &= \sum_{l=1}^{L} \|\mathbf{curl}(\Pi_l - \Pi_{l-1})\boldsymbol{\mu}_h\|^2_{\boldsymbol{L}^2(D)} \\
&\leq C \sum_{l=1}^{L} h_l^{-2} \|(\Pi_l - \Pi_{l-1})\boldsymbol{\mu}_h\|^2_{\boldsymbol{L}^2(D)} \\
&\leq C \left(\sum_{k=1}^{L} h_k^{-2} \|\boldsymbol{\mu}_k\|^2_{\boldsymbol{L}^2(D)} + 2 \sum_{l=1}^{L-1} h_l^{-2} \|\tilde{\boldsymbol{\mu}}_l\|^2_{\boldsymbol{L}^2(D)} \right) \\
&\leq CL^2 \|\mathbf{v}_h\|^2_{\boldsymbol{L}^2(D)},
\end{aligned}$$

and

$$\|I_0 \mathbf{v}_h\|^2_{\boldsymbol{L}^2(D)} = \|\boldsymbol{\mu}_0 + \tilde{\boldsymbol{\mu}}_0\|^2_{\boldsymbol{L}^2(D)} \leq CL^2 \|\mathbf{v}_h\|^2_{\boldsymbol{L}^2(D)}.$$

Please note that mere scaling of D does not affect the constant in the previous estimate. This leads to a dependence of C only on the angles of D, but not its size. Next, the considerations can be applied to all elements of $\mathscr{T}_0$.

Finally, if the meshes have been locally refined, the above estimates remain valid; We can formally pad the sequence of meshes with additional elements to obtain a hierarchy of quasi-uniform meshes. However, $\mathbf{v}_h$ is not affected and, thus, the hierarchical surplus on the extra elements vanishes. □

We are now in a position to prove the main result of this section:

Theorem 4 (Stability of multilevel gauging). *Write* $\boldsymbol{\xi}_h \in \mathscr{NL}_1(\Omega;\mathscr{T}_L)$ *for the vector potential of* $\mathbf{v}_h \in \mathscr{RT}_0^0(\Omega;\mathscr{T}_L)$ *obtained through multilevel gauging. Then*

$$\|\boldsymbol{\xi}_h\|_{\boldsymbol{L}^2(\Omega)} \leq CL\|\mathbf{v}_h\|_{\boldsymbol{L}^2(\Omega)}.$$

Proof: Recall the definition of $\boldsymbol{\xi}_k \in \mathscr{NL}_1(\Omega;\mathscr{T}_k)$, $k \geq 1$ from (14). We zero in on a single macro-element $\mathbf{T} \in \hat{\mathscr{T}}_{k-1}$. From the discussion of the algorithm it is clear that the d.o.f. of $\boldsymbol{\xi}_k$ located in $\mathbf{T}$ are calculated from those of $\mathbf{v}_k \in \mathscr{RT}_0^0(\Omega;\mathscr{T}_k)$ from (7) by a linear mapping. This very linear mapping does only depend on the refinement template applied to $\mathbf{T}$. Thus, for the vectors of d.o.f. on $\mathbf{T}$ and then for all degrees of freedom we get

$$|\vec{\boldsymbol{\xi}}_{k|\mathbf{T}}| \leq C|\vec{\mathbf{v}}_{k|\mathbf{T}}| \quad \Longrightarrow \quad \|\boldsymbol{\xi}_k\|_{\boldsymbol{L}^2(\mathbf{T})} \leq Ch_{\mathbf{T}}\|\mathbf{v}_k\|_{\boldsymbol{L}^2(\mathbf{T})}, \tag{20}$$

with $C > 0$ only depending on the refinement template and shape regularity of $\mathbf{T}$. Now, let h_k denote the average size of elements in $\tilde{\mathscr{T}}_k$ and recall that supp $\mathbf{v}_k \subset \cup\{T \in \tilde{\mathscr{T}}_k\}$. We conclude

$$\|\boldsymbol{\xi}_k\|_{\boldsymbol{L}^2(\Omega)} \leq Ch_k\|\mathbf{v}_k\|_{\boldsymbol{L}^2(\Omega)}.$$

We know that h_k shrinks geometrically as k increases. Thus, using (20) and the result of Theorem 3, we get, with $\mathbf{v}_k := (I_k - I_{k-1})\mathbf{v}_h$,

$$\|\boldsymbol{\xi}_h\|^2_{\boldsymbol{L}^2(\Omega)} \leq \left(\sum_{k=0}^{L}\|\boldsymbol{\xi}_k\|_{\boldsymbol{L}^2(\Omega)}\right)^2 \leq C\left(\sum_{k=0}^{L}h_k^2\right)\left(\sum_{k=0}^{L}\|\mathbf{v}_k\|^2_{\boldsymbol{L}^2(\Omega)}\right) \leq CL^2\|\mathbf{v}_h\|^2_{\boldsymbol{L}^2(\Omega)}.$$

This finishes the proof. □

The last theorem bears out the superior stability of multilevel gauging compared to co-tree gauging, though the stability achieved is only suboptimal.

The discussion of stability for the higher order case is not a big deal. For second order Raviart–Thomas elements the L^2-stability of the bases tells us that the higher order components from (16) and (17) satisfy

$$\|\boldsymbol{\xi}_h^{(1)}\|_{\boldsymbol{L}^2(\Omega)} \leq C\|\mathbf{v}_h^{(1)}\|_{\boldsymbol{L}^2(\Omega)},$$

with $C > 0$ only depending on the (uniform) shape regularity measure of the meshes. In sum, the estimate of Theorem 3 carries over.

6. Impact of Perturbations

Often only an approximation $\tilde{\mathbf{v}}_h$ of $\mathbf{v}_h \in \mathscr{RT}_0^0(\Omega;\mathscr{T}_L)$ is known, either due to the truncation error of some iterative scheme or due to numerical quadrature. As $\operatorname{div}\tilde{\mathbf{v}}_h = 0$ does no longer hold exactly, we have to figure out how a lack of solenoidality affects the computed "vector potential" $\tilde{\boldsymbol{\xi}}_h$. Note that, barring a

breakdown on level 0, the algorithm will provide us with a $\tilde{\boldsymbol{\xi}}_h$, regardless whether $\tilde{\mathbf{v}}_h$ is solenoidal or not. This "robustness" of the computation of $\boldsymbol{\xi}_0$ is, e.g., present with the saddle point problem (15).

A generalization of Theorem 3 is the key to gauging the effect of a non-solenoidal perturbation on $\tilde{\boldsymbol{\xi}}_h$:

Theorem 5 (Stability of hierarchical splitting of face element space). *For all* $\mathbf{w}_h \in \mathscr{RT}_0(\Omega;\mathscr{T}_L)$ *holds*

$$\|I_0\mathbf{w}_h\|^2_{\boldsymbol{L}^2(\Omega)} + \sum_{k=1}^{L}\|(I_k - I_{k-1})\mathbf{w}_h\|^2_{\boldsymbol{L}^2(\Omega)} \leq CL^2\|\mathbf{w}_h\|^2_{\boldsymbol{H}(\mathrm{div};\Omega)},$$

with a constant $C > 0$ *only depending on the shape regularity of the meshes.*

Proof: As in the proof of Theorem 3 we first assume uniform refinement and consider a single coarse grid element $D \in \mathscr{T}_0$. Taking the cue from Theorem 2, we start with the decompositions

$$\begin{aligned}
&\mathbf{w}_h = \mathbf{v}_h + \mathbf{q}_h, \quad \mathrm{div}\,\mathbf{v}_h = 0, \quad \mathbf{v}_h, \mathbf{q}_h \in \mathscr{RT}_0(D;\mathscr{T}_L),\\
&\mathbf{q}_h = \sum_{k=0}^{L}\mathbf{q}_k, \quad \mathbf{q}_k \in \mathscr{RT}_0(\Omega;\mathscr{T}_k).
\end{aligned}$$

The stability for the hierarchical decomposition of $\mathbf{v}_h$ has already been dealt with in the proof of Theorem 3. In addition, we make use of $\|\mathbf{v}_h\|_{\boldsymbol{L}^2(D)} \leq C\|\mathbf{w}_h\|_{\boldsymbol{H}(\mathrm{div};D)}$. Similarly as in the proof of Theorem 3, we tackle $\mathbf{q}_h$:

$$(I_l - I_{l-1})\mathbf{q}_h = \mathbf{q}_l + \underbrace{I_l\left(\sum_{k=l+1}^{L}\mathbf{q}_k\right)}_{=:\tilde{\mathbf{q}}_l} - \underbrace{I_l\left(\sum_{k=l}^{L}\mathbf{q}_k\right)}_{=:\tilde{\mathbf{q}}_{l-1}}.$$

Using part (ii) of Lemma 1, we can proceed as above

$$\begin{aligned}
\sum_{l=0}^{L-1}\|\tilde{\mathbf{q}}_l\|^2_{\boldsymbol{L}^2(D)} &\leq C\sum_{l=0}^{L-1}h_l^{-1}\sum_{F\in\mathscr{F}_l^D}\kappa_F(\tilde{\mathbf{q}}_l)^2 \leq C\sum_{l=0}^{L-1}h_l^{-1}\sum_{F\in\mathscr{F}_l^D}\left(\sum_{k=l+1}^{L}\kappa_F(\mathbf{q}_k)\right)^2\\
&\leq C\sum_{l=0}^{L-1}h_l^{-1}\sum_{F\in\mathscr{E}_l}(L-l-1)\sum_{k=l+1}^{L}h_l^2h_k^{-1}\|\mathbf{q}_k\|^2_{\boldsymbol{L}^2(\omega_{F,k})}\\
&\leq C\sum_{l=0}^{L-1}\sum_{k=l+1}^{L}h_k^{-1}h_l(L-l-1)\|\mathbf{q}_k\|^2_{\boldsymbol{L}^2(D)}\\
&\leq C\sum_{k=1}^{L}h_k^{-1}\|\mathbf{q}_k\|^2_{\boldsymbol{L}^2(D)} \leq C\|\mathbf{q}_h\|^2_{\boldsymbol{H}(\mathrm{div};D)} \leq C\|\mathbf{w}_h\|^2_{\boldsymbol{H}(\mathrm{div};D)}.
\end{aligned}$$

The remainder of the proof follows the lines of the proof of Theorem 3 and will be omitted. □

Remark. A different approach to proving the Theorems 3 and 5, already successful in 2D [49], could set out from [50, Lemma 4.1].

Corollary 1 (Impact of non-solenoidal perturbation). *For a general* $\mathbf{w}_h \in \mathscr{R}\mathscr{T}_0(\Omega;\mathscr{T}_L)$ *the "vector potential"* $\boldsymbol{\xi}_h \in \mathscr{N}\mathscr{D}_1(\Omega;\mathscr{T}_L)$ *computed by multilevel gauging with a robust coarse grid procedure satisfies*

$$\|\boldsymbol{\xi}_h\|_{\boldsymbol{L}^2(\Omega)} \leq CL\|\mathbf{v}_h\|_{\boldsymbol{H}(\mathrm{div};\Omega)},$$

with a constant $C > 0$ *only depending on the shape regularity of the meshes*

Example. Imagine that the degrees of freedom for $\mathbf{w}_h \in \mathscr{R}\mathscr{T}_0(\Omega;\mathscr{T}_L)$ have been computed by one-point Gaußian quadrature from the face fluxes of a C^2-smooth solenoidal vector field $\mathbf{j}$. Then, in general, $\mathbf{w}_h = I_L\mathbf{j} + \mathbf{d}_h$ with some quadrature error $\mathbf{d}_h \in \mathscr{R}\mathscr{T}_0(\Omega;\mathscr{T}_L)$. Provided that the meshes are quasi-uniform we can expect $\kappa_F(\mathbf{d}_h) := \int_F \langle \mathbf{j}, \mathbf{n}\rangle d\sigma - |F|\langle \mathbf{j}(\mathbf{m}_F), \mathbf{n}\rangle$ ($F \in \mathscr{F}_L$ with center of gravity $\mathbf{m}_F$) to be of the asymptotic order $O(h_L^4)$. For $T \in \mathscr{T}_L$ Gauß' theorem yields (the sign determined by the orientation of the faces)

$$\mathrm{div}\,\mathbf{d}_{|T} = |T|^{-1} \cdot \sum_{F\in\mathscr{F}_L, F\subset\partial T} \pm\kappa_F(\mathbf{d}).$$

This shows that $\|\mathrm{div}\,\mathbf{d}\|_{\boldsymbol{L}^2(\Omega)} = O(h_L)$, too. Thus, the spurious part $\boldsymbol{\delta}_h$ of the vector potential obtained through multilevel gauging, satisfies $\|\boldsymbol{\delta}_h\|_{\boldsymbol{L}^2(\Omega)} = O(Lh_L)$, which means that there is no significant impact of the quadrature error.

7. Numerical Experiments

The asymptotic theoretical estimates are littered with elusive constants. Numerical experiments are the only way to get an idea about their sizes in particular settings.

All numerical experiments reported in this paper rely on lowest order finite elements on uniformly refined hexahedral grids. The elements of $\mathscr{T}_l$ are cubes of meshwidth $h_l = 2^{-(l+1)}$. The vector potential on the coarses grid $\mathscr{T}_0$ is determined by solving a saddle point problem similar to (15).

In the experiments we estimate the operator norm

$$\|G_h\| := \sup\{\|G(\mathbf{v}_h)\|_{\boldsymbol{L}^2(\Omega)},\ \mathbf{v}_h \in \mathscr{R}\mathscr{T}_0^0(\Omega;\mathscr{T}_L),\ \|\mathbf{v}_h\|_{\boldsymbol{H}(\mathrm{div};\Omega)} = 1\}$$

for the linear operator $G_h : \mathscr{R}\mathscr{T}_0^0(\Omega;\mathscr{T}_L) \mapsto \mathscr{N}\mathscr{D}_1(\Omega;\mathscr{T}_L)$ of multilevel gauging. Beside the true value of $\|G_h\|$, we are mainly interested in its dependence on the

Table 1. Computed norms $\|G_h\|$ of multilevel gauging operator in experiments #1 through #4

Exp. \ L	2	3	4	5	6
#1	0.37	0.42	0.47	0.51	0.55
#2	0.47	0.54	0.61	0.67	0.73
#3	0.36	0.39	0.43	0.46	0.50
#4	0.47	0.55	0.61	0.67	0.73

depth L of the multilevel hierarchy (cf. Theorem 3). In order to compute $\|G_h\|$ we resort to the generalized eigenvalue problem: Seek $\vec{\boldsymbol{\xi}}_h \neq 0$ and $\lambda > 0$ such that

$$\mathbf{curl}_h^T \, G_h^T M_h^{\mathcal{N}\mathcal{D}} G_h \mathbf{curl}_h \, \vec{\boldsymbol{\xi}}_h = \lambda \, \mathbf{curl}_h^T \, M_h^{\mathcal{R}\mathcal{T}} \mathbf{curl}_h \, \vec{\boldsymbol{\xi}}_h. \tag{21}$$

Here, $\mathbf{curl}_h$ is the matrix of the discrete **curl** operator, $M_h^{\mathcal{N}\mathcal{D}}$ and $M_h^{\mathcal{R}\mathcal{T}}$ stand for the finite element mass matrices, and T labels the adjoint w.r.t. the Euclidean inner product. The maximal eigenvalue $\lambda_{\max}$ of (21) can be found by means of a non-linear CG method applied to the generalized Rayleigh quotient [46]. The iterations terminate, when the value for the Rayleigh quotient becomes almost (up to a relative change $< 10^{-5}$) stationary.

In the first experiment (#1) we use $\Omega :=]0;1[^3$ and impose homogeneous Dirichlet boundary conditions on $\partial\Omega$. The second experiment (#2) is carried out on the same domain, but with free boundary values. The domain used in the third experiment (#3) is a three-dimensional "L-shaped" domain $\Omega_L :=]0;1[^3 \backslash [0;\frac{1}{2}]^3$. Zero boundary values for the functions are specified. Finally, the fourth experiment (#4) retains the domain Ω_L, but allows free boundary values.

The norms $\|G_h\|$ obtained from the experiments are recorded in Table 1. The figures indicate that the constants are of moderate size for the problem investigated numerically. They also give evidence that the shape of the domain does not make a big difference. In addition, an affine-linear dependence of $\|G_h\|$ on the depth L of refinement is evident. Thus, the theoretical estimates seem to be sharp.

8. Conclusion

In this paper a new method for calculating a discrete vector potential for a solenoidal vector field in Raviart–Thomas finite element space has been developed. It can be profitably employed if multilevel data structures are available. In contrast to co-tree gauging, the new method comes up with a vector potential whose norm is neatly bounded by the norm of its **curl** times the number of grid levels employed times a constant depending on shape regularity. It does so with minimal computational effort.

References

[1] Albanese, R., Rubinacci, G.: Integral formulation for 3D eddy-current computation using edge elements. IEE Proc. A *135*, 457–462 (1988).

[2] Albanese, R., Rubinacci, G.: Fomulation of the eddy-current problem. IEE Proc. A *137*, 16–22 (1990).
[3] Amrouche, C., Bernardi, C., Dauge, M., Girault, V.: Vector potentials in three-dimensional nonsmooth domains. Math. Methods Appl. Sci. *21*, 823–864 (1998).
[4] Arnold, D., Falk, R., Winther, R.: Multigrid in $H(\mathrm{div})$ and $H(\mathbf{curl})$. Numer. Math. (2000) (to appear).
[5] Arnold, D., Mukherjee, A., Pouly, L.: Locally adapted tetrahedral meshes using bisection. SIAM J. Sci. Comput. (2000) (to appear).
[6] Bank, R.: Hierarchical bases and the finite element method. Acta Numer. *5*, 1–43 (1996).
[7] Bank, R., Dupont, T., Yserentant, H.: The hierarchical basis multigrid method. Numer. Math. *52*, 427–458 (1988).
[8] Bänsch, E.: Local mesh refinement in 2 and 3 dimensions. IMPACT Comput. Sci. Eng. *3*, 181–191 (1991).
[9] Bastian, P., Birken, K., Johannsen, K., Lang, S., Neuss, N., Rentz-Reichert, H., Wieners, C.: UG-A flexible software toolbox for solving partial differential equations. Comput. Visual. Sci. *1*, 27–40 (1997).
[10] Beck, R., Deuflhard, P., Hiptmair, R., Hoppe, R., Wohlmuth, B.: Adaptive multilevel methods for edge element discretizations of Maxwell's equations. Surv. Math. Ind. *8*, 271–312 (1999).
[11] Beck, R., Erdmann, B., Roitzsch, R.: KASKADE 3.0. An object-oriented adaptive finite element code. Tech. Rep. TR 95-4, ZIB, Berlin, Germany, June 1995.
[12] Beck, R., Hiptmair, R., Hoppe, R., Wohlmuth, B.: A hierarchical error estimator for $H(\mathrm{curl})$-elliptic problems. Tech. Rep. 112, Sonderforschungsbereich 382, Universität Tübingen, Tübingen, Germany, 1998. To appear in $\mathrm{M}^2\mathrm{AN}$.
[13] Bey, J.: Tetrahedral grid refinement. Computing *55*, 355–378 (1995).
[14] Biro, O., Richter, K.: CAD in electromagnetism. In: Advances in Electronics and Electron Physics, vol. 82 (Hawkes, P., ed.) pp. 1–96. New York: Academic Press, 1991.
[15] Bossavit, A.: A rationale for edge elements in 3D field computations. IEEE Trans. Mag. *24*, 74–79 (1988).
[16] Bossavit, A.: Whitney forms: A class of finite elements for three-dimensional computations in electromagnetism. IEE Proc. A *135*, 493–500 (1988).
[17] Bossavit, A.: Computational electromagnetism. Variational formulation, complementarity, edge elements. Academic Press Electromagnetism Series, vol. 2. Academic Press, San Diego, 1998.
[18] Brandt, A.: Multigrid techniques: 1984 guide with applications, of GMD-Studien, vol. 85. Bonn: GMD, 1984.
[19] Brezzi, F., Fortin, M.: Mixed and hybrid finite element methods. Berlin Heidelberg New York Tokyo: Springer, 1991.
[20] Cendes, C., Shenton, D.: Adaptive mesh refinement in the finite element computation of magnetic fields. IEEE Trans. Mag. *21*, 1811–1816 (1985).
[21] Ciarlet, P.: The finite element method for elliptic problems. Studies in Mathematics and its Applications, vol. 4 North-Holland, Amsterdam, 1978.
[22] Ciarlet, P., Jr., Zou, J.: Fully discrete finite element approaches for time-dependent Maxwell equations. Numer. Math. *82*, 193–219 (1999).
[23] Dubois, F.: Discrete vector potential representation of a divergence free vector field in three dimensional domains: Numerical analysis of a model problem. SIAM J. Numer. Anal. *27*, 1103–1141 (1990).
[24] Dular, P., Hody, J.-Y., Nicolet, A., Genon, A., Legros, W.: Mixed finite elements associated with a collection of tetrahedra, hexahedra and prisms. IEEE Trans. Magnetics, MAG-30, 2980–2983 (1994).
[25] Erdmann, B., Lang, J., Roitzsch, R.: Kaskade manual, version 2.0 – fem for 2 and 3 space dimensions. Tech. Rep. TR 93-5, ZIB-Berlin, 1993.
[26] Ewing, R., Wang, J.: Analysis of the Schwarz algorithm for mixed finite element methods. $\mathrm{M}^2\mathrm{AN}$ Math. Modell. Numer. Anal. *26*, 739–756 (1992).
[27] Girault, V., Raviart, P.: Finite element methods for Navier–Stokes equations. Berlin Heidelberg New York Tokyo: Springer, 1986.
[28] Gradinaru, V., Hiptmair, R.: Discrete differential forms for pyramidal elements. Tech. Rep. 113, SFB 382, Universität Tübingen, Tübingen, Germany, 1999.
[29] Graglia, R., Wilton, D., Peterson, A.: Higher order interpolatory vector bases for computational electromagnetics. IEEE Trans. Antennas and Propagation *45*, 329–342 (1997).
[30] Hackbusch, W.: Multi-grid methods and applications. Berlin Heidelberg New York Tokyo: Springer, 1985.
[31] Hiptmair, R.: Multigrid method for $H(\mathrm{div})$ in three dimensions. ETNA *6*, 7–77 (1997).

[32] Hiptmair, R.: Canonical construction of finite elements. Math. Comp. *68*, 1325–1346 (1999).
[33] Hiptmair, R.: Multigrid method for Maxwell's equations. SIAM J. Numer. Anal. *36*, 204–225 (1999).
[34] Hiptmair, R., Hoppe, R.: Multilevel preconditioning for mixed problems in three dimension. Numer. Math. *82*, 253–279 (1999).
[35] Hiptmair, R., Toselli, A.: Overlapping and multilevel Schwarz methods for vector valued elliptic problems in three dimensions. In: Parallel Solution of PDEs, IMA Volumes in Mathematics and its Applications, Vol. 120 (Bjorstad, P., Luskin, M., eds.), pp. 181–202. Berlin Heidelberg New York Tokyo: Springer, 1999.
[36] Jackson, J.: Classical Electrodynamics. Wiley, New York, 2nd ed., 1975.
[37] Kettunen, L., Forsman, K., Bossavit, A.: Formulation of the eddy current problems in multiply connected regions in terms of **h**. Int. J. Numer. Meth. Eng. *41*, 935–954 (1998).
[38] Kettunen, L., Forsman, K., Bossavit, A.: Gauging in Whitney spaces. IEEE Trans. Magnetics *35*, 1466–1469 (1999).
[39] Leinen, P.: Data structures and concepts for adaptive finite element methods. Computing *55*, 325–354 (1995).
[40] Mitchell, W.: Optimal multilevel iterative methods for adaptive grids. SIAM J. Sci. Stat. Comput. *13*, 146–167 (1992).
[41] Nédélec, J.: Mixed finite elements in R^3. Numer. Math. *35*, 315–341 (1980).
[42] Peng, G., Dyczij-Edlinger, R., Lee, J.-F.: Hierarchical methods for solving matrix equations from TVFEMs for microwave components. IEEE Trans. Mag. *35*, 1474–1477 (1998).
[43] Perugia, I.: A mixed formulation for 3D magnetostatic problems: Theoretical analysis and face-edge finite element approximation. Numer. Math. (1999) (online).
[44] Raviart, P. A., Thomas, J. M.: A mixed finite element method for second order elliptic problems. Springer Lecture Notes in Mathematics, vol. 606, pp. 292–315. New York: Springer, 1977.
[45] Savage, J., Peterson, A.: Higher order vector finite elements for tetrahedral cells. IEEE Trans. Microwave Theory Technol. *44*, 874–879 (1996).
[46] Schwarz, H.: Methode der finiten Elemente. 3. Aufl. Leitfäden der angewandten Mathematik und Mechanik, vol. 47, Stuttgart: Teubner B. G., 1991.
[47] Subramaniam, S., Ratnajeevan, S., Hoole, S.: Edge elements. In: Finite Elements, Electromagnetics and Design, (Hoole, S., Ratnajeevan, S., eds.), pp. 342–393. Amsterdam: Elsevier, 1995.
[48] Verfürth, R.: A review of a posteriori error estimation and adaptive mesh-refinement techniques. Teubner-Verlag, Stuttgart, 1996.
[49] Wohlmuth, B.: Adaptive Multilevel-Finite-Elemente Methoden zur Lösung elliptischer Randwertprobleme. PhD thesis, TU München, 1995.
[50] Wohlmuth, B., Toselli, A., Widlund, O.: An iterative substructuring method for Raviart–Thomas vector fields in three dimensions. Tech. Rep. 773, Courant Institute, New York, 1998.
[51] Yserentant, H.: On the multi-level splitting of finite element spaces. Numer. Math. *58*, 379–412 (1986).

Dr. Ralf Hiptmair
Sonderforschungsbereich 382
Universität Tübingen
Auf der Morgenstelle 10
D-72076 Tübingen
Germany
e-mail: hiptmair@na.uni-tuebingen.de